CFD Simulation of UV Photocatalytic Reactors for Air Treatment

Fariborz Taghipour and Madjid Mohseni
Dept. of Chemical and Biological Engineering, University of British Columbia, Vancouver, BC V6T 1Z4, Canada

DOI 10.1002/aic.10538
Published online August 3, 2005 in Wiley InterScience (www.interscience.wiley.com).

A photocatalytic reactor was simulated through computational fluid dynamics (CFD) with surface reaction for trichloroethylene (TCE) oxidation at various pollutant concentrations, flow rates, and reactor lengths. The results were compared with those from experiments. The experimental work involved using a differential photoreactor for kinetics studies and an annular flow photoreactor for overall removal investigations under various conditions. The modeling predictions agreed closely with the experimental data within the range in which results were examined. The modeling results indicated significant radial TCE concentration gradient and nonuniform flow distributions in the annular photoreactor. CFD was applied to predict the performance of a number of UV photocatalytic reactor design concepts, to study the impacts of some design parameters on the reactor efficiency. The modeling results demonstrated that under similar flow rate conditions, the thickness of the contaminated air layer flowing over the photocatalyst surface could substantially influence the reactor performance. Thinner contaminated air layers provided more uniform radial concentration distribution of TCE and improved the reactor performance. © 2005 American Institute of Chemical Engineers *AIChE J,* 51: 3039–3047, 2005
Keywords: CFD, photocatalysis, trichloroethylene (TCE), UV, air treatment

Introduction

Heterogeneous photocatalysis, using semiconductor particles such as TiO_2 in combination with ultraviolet (UV) irradiation, has proved to be very effective for the abatement of contaminated air streams.[1-3] This effectiveness along with the increasingly stringent environmental regulations has intensified research toward the development of efficient photoreactors for large-scale applications. To that end many researchers have investigated different photoreactor configurations for air treatment,[1,4-6] and have attempted to understand the fundamentals of photoreactor design and development using mathematical modeling.[2,5] More recently, computational fluid dynamics (CFD) has been used as a tool to simulate photoreactor performance.[7,8]

CFD, which uses the conservation of mass and momentum equations to model fluid flow, is a valuable tool for simulating reacting flows with high precision. It is often superior to simplified hydrodynamic models, such as plug flow or completely mixed, which do not usually reflect the real flow pattern inside the reactors. By incorporating detailed description of flow in complex reactor geometries using CFD, the use of plug-flow or completely mixed assumptions and correlations for mass transfer can be avoided. In simulating reactive flows, in addition to mass and momentum equations, the mixing, transport, and production/consumption of chemical species should also be considered through species transport equations, which represent the conservation of each species in the system. The system of equations is solved in the computational domain using one of the numerical techniques (such as finite-volume).

CFD has been applied to modeling fluid flow and overall performance of single-phase and multiphase chemical reactors,[9-12] as well as photoreactors. In photoreactors with volumetric reactions, such as UV disinfection or oxidation reactions, reaction kinetics is usually a function of radiation fluence rate. As a result, radiation models describing the fluence rate distribution are required for considering the radiation effect on reactor performance. In modeling photoreactors, the reaction

Correspondence concerning this article should be addressed to F. Taghipour at fariborz@chml.ubc.ca.

kinetics and radiation distribution are integrated with the reactor hydrodynamics to predict reactor performance. Kucuk Unluturk et al.[13] performed CFD modeling of the UV dose distribution in a thin-film UV reactor for processing of apple cider, and observed reasonable agreement between simulation and experimental UV dose values. Pareek et al.[7] conducted CFD modeling of a three-phase photocatalytic reactor using an Eulerian–Eulerian approach and reported on the model adequacy for predicting the experimental results and reactor performance. Models for simulating the performance of ozone-UV reactors[14] and UV disinfection reactors[15] have been developed, taking into account parameters such as kinetics, hydrodynamics, and fluence rate within the reactor. The results indicated that decomposition of contaminants is influenced by both reactor hydrodynamics and fluence rate distribution.

CFD has also been applied to simulate surface reactions in catalytic reactors. Endo et al.[16] presented a CFD model for the rate of carbon nanotubes production by catalytic decomposition of xylene in a chemical vapor deposition reactor. Using gas-phase and surface reactions, the authors reported good agreement of the model with the experimental data. Seo et al.[17] carried out CFD simulation of the surface reactions of a catalytic heat exchanger and found reasonable agreement between the modeling and experimental results. Heitsch[18] performed CFD analysis of catalytic surface reactions in a catalytic recombiner and compared the results with the reported test data. Finally, in a study of photocatalytic destruction of gas-phase vinyl chloride (VC), Mohseni and Taghipour[8] demonstrated that both CFD modeling and experimental approaches showed similar trends with respect to VC removal as a function of VC loading rate.

The primary objectives of this study were: to evaluate CFD's capability in modeling the performance of UV photocatalytic reactors for use in air treatment; to use CFD to provide a better understanding of the flow characteristics and their impacts on the overall reactor performance; and to explore CFD application as a tool for improving photoreactor design. The performance of a UV photocatalytic reactor was predicted by CFD and the results were compared with those from experiments under various pollutant concentrations, gas flow rates, and reactor lengths. CFD was also applied to predict the performance of a few UV photocatalytic reactor design concepts to study the impacts of some design parameters on the reactor efficiency.

CFD Modeling

The transport and chemical reactions were modeled by solving mass, momentum, and species conservation equations, using Fluent 6.0 CFD software.[19] The simulation of the system was performed with a three-dimensional, steady-state, laminar-flow model including the photocatalytic surface reaction.[19] The general forms of the governing equations for modeling the system are as follows:

Conservation of Mass

$$\frac{\partial \rho}{\partial t} + \nabla \cdot (\rho \vec{v}) = 0 \tag{1}$$

Conservation of Momentum

$$\frac{\partial (\rho v)}{\partial t} + \nabla \cdot (\rho v \vec{v}) = -\nabla P + \nabla \cdot (\bar{\bar{\tau}}) + \rho g \tag{2}$$

Conservation of Species Y_i

$$\frac{\partial (\rho Y_i)}{\partial t} + \nabla \cdot (\rho \vec{v} Y_i) = -\nabla \cdot \vec{J}_i + R_i \tag{3}$$

In Eqs. 1–3, ρ is density, $\vec{v}$ is velocity, P is pressure, $\bar{\bar{\tau}}$ is stress tensor, g is gravitational force, and $\vec{J}_i$ is diffusion flux of species i. In the species equation (Eq. 3), in addition to "convective" and "diffusive" terms, the "reactive" term also appears. In this equation, R_i is the rate of production or depletion of the compounds by chemical reaction.

Reactions may occur at the photoreactor wall surface and/or in the homogeneous phases. For surface reaction, the concentration of the species on reacting surface is based on a balance between the convection/diffusion of each species to/from the surface and the consumption/production rate at the surface:

$$\vec{J}_i \cdot \vec{n} = R_i^s \tag{4}$$

where $\vec{n}$ is a unit vector normal to the surface and R_i^s is the rate of the production/depletion of species i arising from surface reaction.

$$R_i^s = M_{w,i} \sum_{r=1}^{N_R} \hat{R}_{i,r}^s \tag{5}$$

where $M_{w,i}$ is the molar weight of the species i and $\hat{R}_{i,r}^s$ is the rate of production/depletion of species i in surface reaction r. R_i^s is computed as the sum of the reaction sources over N_R reactions in which the species i is involved.

The general form of the rth surface reaction can be considered as

$$\sum_{i=1}^{N} \nu'_{i,r} M_i \xrightarrow{k_{f,r}} \sum_{i=1}^{N} \nu''_{i,r} M_i \tag{6}$$

where N is the total number of species in the system, $\nu'_{i,r}$ is the stoichiometric coefficient for reactant i in reaction r, $\nu''_{i,r}$ is the stoichiometric coefficient for product i in reaction r, M_i is the symbol denoting species i, and $k_{f,r}$ is the forward rate constant for reaction r.

The molar rate of production/depletion of species i in reaction r, $\hat{R}_{i,r}^s$, is given by

$$\hat{R}_{i,r}^s = (\nu'_{i,r} - \nu''_{i,r}) \left(k_{f,r} \sum_{j=1}^{N_r} [C_{j,r}]^{\eta'_{j,r}} \right) \tag{7}$$

where N_r is the number of chemical species in reaction r, $C_{j,r}$ is the molecular concentration of each reactant and product species j in reaction r, and $\eta'_{j,r}$ is the forward rate exponent for each reactant and product species j in reaction r.

In the vapor phase, trichloroethylene (TCE) absorbs UV

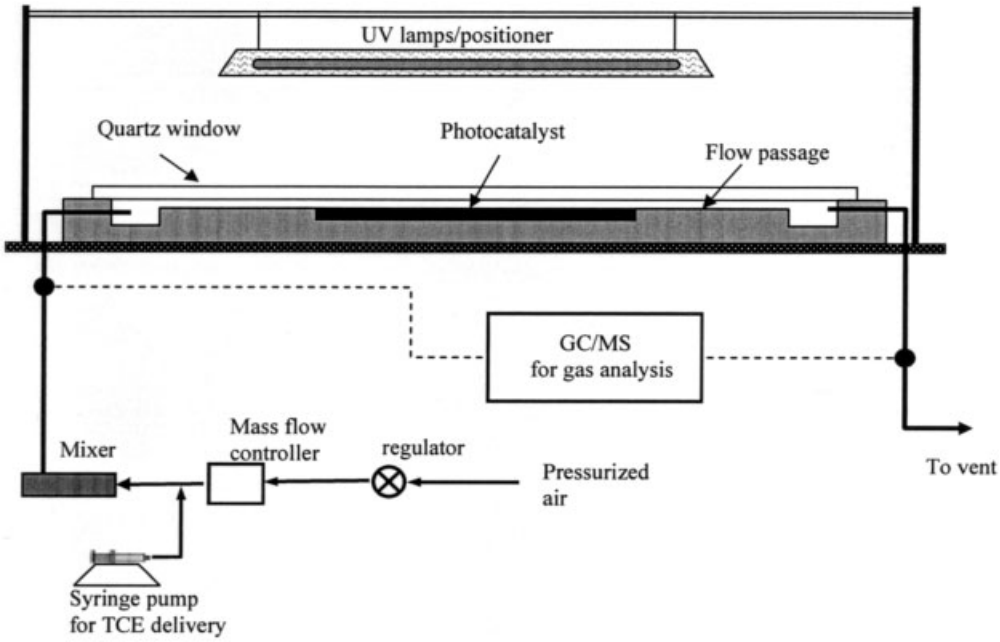

Figure 1. Glass plate differential photoreactor.

slightly ($\sim$1000 M^{-1} m^{-1}) at a wavelength of 254 nm,[20] and thus the homogeneous photolytic reaction in the photoreactors irradiated by 254-nm lamps was insignificant. This was further substantiated in our research, where photolytic experiments conducted with no photocatalyst present in the photoreactor, showed that UV photolysis provided $<$5% TCE removal from the contaminated air. Given this insignificant contribution, heterogeneous photocatalysis on the wall surface (R_i^s) was the primary reaction that took place in the system. Thus, the following one-step reaction on the surface of the photocatalyst was considered

$$C_2HCl_3\ (\text{gas phase}) \rightarrow C_2HCl_3\ (\text{surface}) \tag{8}$$

$$C_2HCl_3\ (\text{surface}) + {}^{\bullet}OH \rightarrow \text{products}_{(CO2+H2O+HCl+\text{intermediates})} \tag{9}$$

The overall degradation of TCE, involving adsorption to the photocatalyst surface followed by the oxidation reaction, was assumed to follow a first-order kinetics. This assumption was supported by the experimental results obtained from the differential glass plate photoreactor (refer to Experimental section). Thus, the molar rate of TCE degradation in the system ($\hat{R}_{i,r}^s$ in Eq. 7) is given by

$$\hat{R}_{i,r}^s = k[C_2HCl_3] \tag{10}$$

where $[C_2HCl_3]$ is the molar concentration of TCE.

The "laminar finite rate" model, in which the transport equations are solved for species mass fractions with the predefined chemical reaction mechanism, was chosen for reaction modeling. The reaction rates appear as reactive terms in the species conservation equations. Models of this type are suitable for simulating a broad range of reacting systems. The Reynolds number for the reactor at the highest air flow rate of 3×10^{-4} m^3 s^{-1} was about 500, which is within the laminar regime.

The three-dimensional physical domain of the photoreactor was discretized with approximately 42,000 hexahedral and tetrahedral cells. Increasing the number of cells to 100,000 through solution-adaptive mesh refinement changed the concentration results by $<$3%, indicating a reasonable sensitivity of the solution to cell size. Physical and chemical properties of the species (that is, TCE and air as contaminant-carrying medium) were specified for calculating the coefficients of the governing equations. The no-slip boundary condition was selected at the surfaces of the lamp and the reactor. Constant fluid velocity with TCE mass fractions and pressure were specified as boundary conditions for the inlet and outlet flows, respectively. A segregated implicit solution algorithm was used to numerically solve the governing equations. The relative error between two successive iterations was specified with a convergence criterion of 10^{-4} for each scaled residual component of mass, velocity, and TCE concentration.

Experimental

Two types of photoreactor setups were used for the photocatalytic experiments involved in this research (complete descriptions are presented elsewhere[8]). Figure 1 shows the schematic of the glass-plate differential photoreactor used to determine the rate of TCE photocatalytic oxidation. It consisted of a 25-mm-wide aluminum reactor designed to allow the contaminated air to flow over the TiO_2 photocatalyst (Degussa P-25, Degussa AG, Düsseldorf, Germany), that was coated on glass plates and placed in the reactor. The reactor was covered by quartz window; gaskets between the quartz window and the aluminum block created a flow passage of 25 mm (width) $\times$ 3 mm (height) above the photocatalyst glass plates. The amount of TiO_2 coated onto glass slides was about 16 g m^{-2} and the

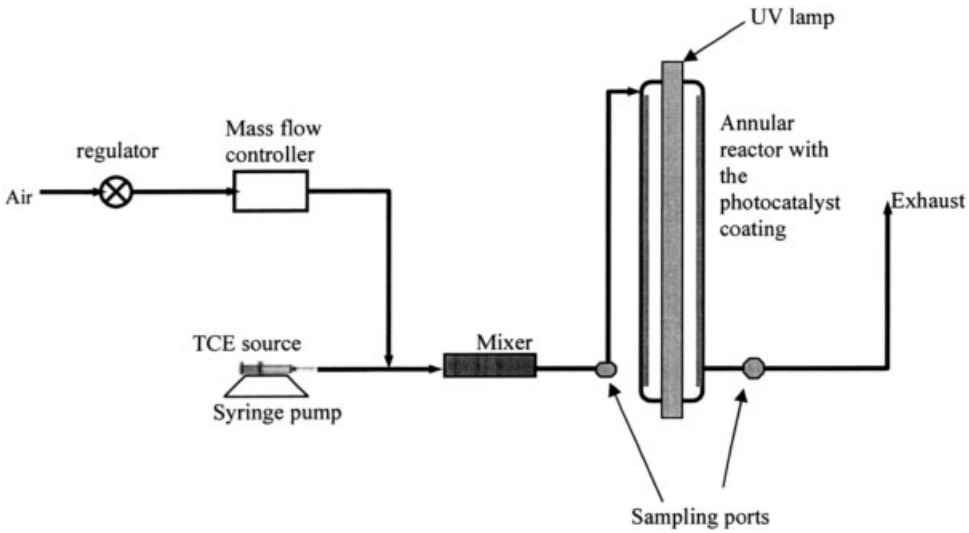

Figure 2. Setup of the annular photoreactor for experimental analysis of TCE photocatalysis.

Annular photoreactor was used for the CFD analysis.

total length of TiO_2-coated slides was 22.5 mm. Two low-pressure monochromatic germicidal lamps (G10T51/2/L, Light Sources Inc., Orange, CT) with 254-nm output, provided UV illumination to the photocatalyst. The UV irradiance was regulated at 30 W m^{-2} by adjusting the distance between the lamps and the catalyst surface. UV irradiance was measured by a radiometer (IL1700, SED240 detector, International Light Inc., Newburyport, MA).

The annular flow photoreactor setup (Figure 2), on which the CFD analysis was conducted, consisted of a glass annular reactor, a mass flow controller, and a syringe pump for delivering TCE. The annular reactor (custom-made, Trojan Technologies Inc., London, Ontario, Canada) was equipped with a UV lamp and a quartz sleeve, which was made of diffused quartz to allow UV to penetrate through and irradiate/activate the TiO_2 photocatalyst (Degussa P-25, Degussa AG) coated on the outside wall of the reactor. Dimensions for the annular reactor were 0.035 m OD, 0.024 m ID (also the OD of the quartz sleeve) and 0.29 m height, with the effective volume of 9×10^{-5} m^3. The UV irradiance in the annular reactor and at the surface of the photocatalyst was constant at 73 W m^{-2} for all experimental runs.

TCE-contaminated air entering the photoreactor was generated using the syringe pump that allowed for the introduction of pure TCE (Fisher certified ACS) into a stream of clean air (pressurized building air) controlled by the mass flow controller (Figures 1 and 2). The retention times and inlet concentrations were adjusted using the mass flow controller for air and the injection rate of the syringe pump, respectively. Covering different portions of the UV lamp in the annular photoreactor allowed one to vary the effective photocatalyst surface area and photoreactor length. This provided an opportunity to run the experiments with different photoreactor lengths while maintaining the same inlet concentrations.

Gas samples were taken from the inlet and outlet streams and were analyzed for the primary contaminant (that is, TCE). Stainless steel tubing (1.6 mm diameter) was used for online samplings from the inlet and outlet streams. Gas analysis was conducted using a gas chromatograph equipped with mass spectrometer detector (GC/MS, Saturn 2200, Varian Associates, Palo Alto, CA) and a megabore capillary column (CPSil-8 CP5860). The injector temperature was 200°C. The initial column temperature was 50°C, held constant for 120 s, after which it was increased to 110°C at a rate of 0.67°C/s. Gas samples were injected into the GC/MS using a six-port sampling/injection valve (Valco Instruments Co., Inc., Houston, TX). A minimum number of three replicate samples were injected.

Results and Discussion

Kinetics of TCE photocatalytic oxidation

The TCE photocatalytic oxidation rate was directly calculated from the change in TCE concentration and gas retention time in the differential glass-plate photoreactor.[8] The effect of mass transfer was investigated by studying the oxidation rate at various air flow rates. At flow rates above 1.4×10^{-4} m^3 s^{-1}, the reaction rate remained constant, indicating that the process was not mass transfer limited. This was in agreement with the results obtained by Keshmiri et al.[21] using the same experimental setup and conditions. To ensure gas-phase mass transfer did not influence the process in further experiments, the oxidation rate was determined at a flow rate of 1.7×10^{-4} m^3 s^{-1}.

Differential mode operation (that is, very low conversion) of the glass-plate photoreactor was confirmed by monitoring the fractional changes of pollutant concentrations that were $<10\%$ for all the experiments. Also, control experiments were conducted without a photocatalyst and under direct photolytic conditions. The results showed no significant oxidation of TCE during the photolysis experiments, indicating that the removals obtained during the photocatalytic oxidation tests were primarily attributed to the presence of TiO_2 and reactions involving OH radicals generated on the surface of the photocatalyst.

Figure 3 shows that the photocatalytic oxidation of TCE on TiO_2 photocatalyst followed first-order kinetics with respect to TCE concentrations up to 1.6 g m^{-3}. These findings agree with

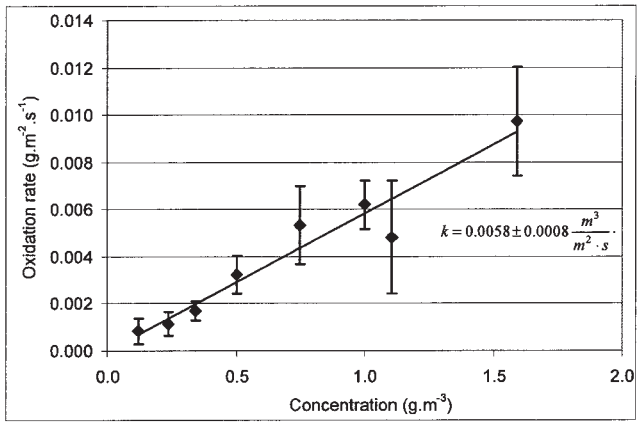

Figure 3. Rate of TCE photocatalytic oxidation as a function of concentration.

Error bars represent the standard deviation for a minimum replication of three samples.

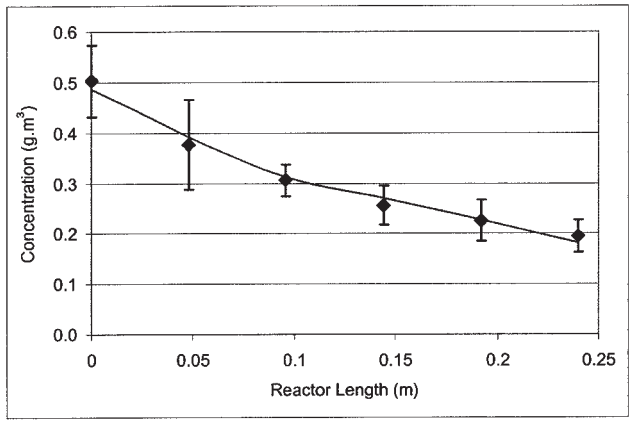

Figure 4. Modeling and experimental results of the concentrations of TCE along the length of the photoreactor (flow rate 1.7 × 10^{-4} m^3 s^{-1}; inlet concentration 0.5 g m^{-3}).

(◆) Represents experimental data; solid line represents CFD simulation. Error bars represent the standard deviation for a minimum replication of three samples.

those of other researchers[2,22] who reported first-order oxidation kinetics for relatively low concentrations of TCE. Because the concentration gradients along the reactor and in reactor cross section are negligible throughout the differential reactor, the rate constant of the surface reaction could be obtained directly from the TCE concentration in the reactor inlet. The kinetic information obtained from the differential reactor was then corrected for the irradiance before being used for the CFD modeling of the annular reactor. This was because the irradiance at the catalyst surface was different for the two reactors as a result of different reactor geometries and configurations. The correction for irradiance from the differential to the annular photoreactor was made based on separate experiments that showed a relatively linear relationship between the reaction rate and irradiance. When the reaction rate constant was corrected for the UV-irradiance difference in the annular and differential reactors, the surface rate constant for the annular photoreactor was 1.2×10^{-2} m^3 m^{-2} s^{-1}.

The first-order dependency of the reaction rate on UV irradiance obtained in this work and used for CFD modeling of the annular photoreactor is in agreement with the literature. Upadhya and Ollis[22] reported that for systems with relatively high photo-efficiency, the rate of TCE photocatalysis follows a first-order irradiance dependency, which is believed to be the result of fairly high gas-phase TCE concentration (between 0.1 and 1.6 g m^{-3}) and high photo-efficiency in the photoreactor.

Comparison between the modeling and experimental results

CFD results were compared to those obtained experimentally for various reactor lengths (0–0.25 m), TCE concentrations (0.08–0.67 g m^{-3}), and flow rates (3×10^{-5}–3×10^{-4} m^3 s^{-1}). Figure 4 compares the CFD-simulated and experimental results for TCE concentrations along the length of the annular photoreactor during photocatalytic oxidation (flow rate 1.7×10^{-4} m^3 s^{-1}, inlet concentration 0.5 g m^{-3}). As expected, the TCE concentration decreases along the photoreactor. The results show a higher initial oxidation rate near the inlet of the photoreactor, which then gradually decreases as the concentration of the pollutant decreases along the length of the reactor. The higher rate near the inlet was accurately predicted by CFD, and is the result of both the higher concentration of TCE in these areas and the first-order kinetics behavior for TCE photocatalysis.

Figure 5 shows the effect of flow rate on TCE degradation at an inlet concentration of approximately 0.5 g m^{-3}. The experimental data indicated that increasing the flow rate (or decreasing the retention time) reduces the percentage of TCE removed, which was predicted by CFD simulation. The relationship between TCE removal and flow rate was to some extent different from that predicted by the first-order oxidation kinetics. Although first-order kinetics behavior predicts an exponential drop in TCE removal with increasing flow rate, a nearly linear relationship was observed at low flow rates. This behavior, observed experimentally and predicted by CFD simulation, could be the result of mass-transfer limitations. At low flow

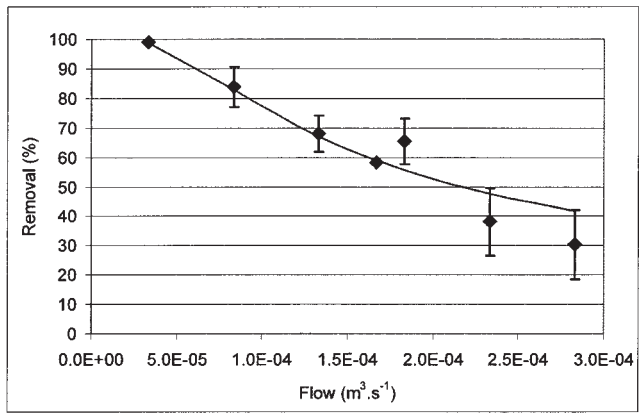

Figure 5. Modeling and experimental results of TCE removal at various flow rates (inlet concentration ≅ 0.5 g m^{-3}).

(◆) Represents experimental data; solid line represents CFD simulation. Error bars represent the standard deviation for a minimum replication of three samples.

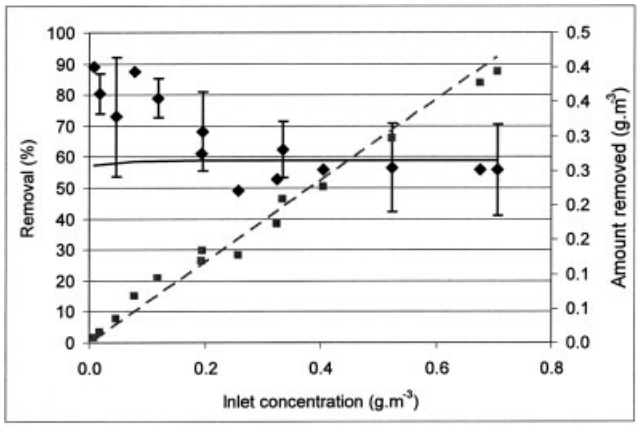

Figure 6. Modeling and experimental results of TCE removal at various concentrations (flow rate 1.7×10^{-4} m^3 s^{-1}).

(◆) Represents experimental data of percentage removal; (■) represents experimental data of amount removed; solid line represents CFD simulation of percentage removal; dashed line represents CFD simulation of amount removed. Error bars represent the standard deviation for a minimum replication of three samples.

rates, there would be a limited degree of radial mixing along the photoreactor that, in turn, prevents TCE molecules that are farther away from the surface boundary layer from reaching the surface of the photocatalyst for adsorption and subsequent degradation. At relatively high gas velocity, increasing the flow rate will induce some degree of turbulence and mixing within certain regions of the photoreactor. Such a phenomenon would increase the diffusion rate of the chemicals to and from the photocatalyst surface. Thus, with reduced mass-transfer limitation at higher flow rates, the percentage removal and reactor behavior approach an exponential shape and the removal rate is less dependent on flow rate.

The removal of TCE at various concentrations is illustrated in Figure 6. Both experimental data and CFD modeling indicate the percentage removal of TCE remains constant at relatively high concentrations (>0.2 g m^{-3}). Such behavior can be explained based on the first-order kinetics for the oxidation of TCE. For first-order kinetics, the rate of oxidation increases with concentration, resulting in higher amounts of TCE removed from the system (Figure 6). This, in turn, corresponds to a relatively constant percentage removal of TCE throughout the range of concentrations between 0.2 and 0.7 g m^{-3}. At concentrations < 0.2 g m^{-3}, however, there is a discrepancy between the CFD modeling and experimental results; the model does not predict the high degree of removal observed experimentally. This difference was likely the result of degradation caused by photolysis that is generally insignificant, especially at higher concentrations. However, when the concentration of TCE decreases and the photocatalytically initiated surface reactions become less pronounced, the small amount of removal obtained by photolysis could become more significant. This hypothesis was further examined using separate photolytic experiments with the glass-plate photoreactor at TCE inlet concentrations of <0.1 g m^{-3}. About 4–5% TCE removal was observed, indicating the potential, albeit small, impact of photolysis to the overall removal of TCE. Given that CFD simulation did not account for homogeneous reactions such as those initiated by photolysis, it showed some deviations from the experimental data at low TCE concentrations (Figure 6).

Overall, Figures 4 through 6 provide an evaluation of the CFD simulation of the photoreactor under various operating conditions. The results demonstrate close agreement between the modeling prediction and the experimental data within the range of reactor lengths, contaminant concentrations, and flow rates that were examined. Such close agreements between CFD predictions and experimental results indicate that CFD could become a valuable tool to understand the system and enhance the design of the photoreactors for optimum photocatalyst activities. Preliminary investigations in this area are presented below.

CFD modeling of different reactor designs

A number of attempts were made to examine the potential for using CFD simulation to improve the photoreactor performance. Different photoreactor configurations and designs were evaluated by studying their effects on reactor hydrodynamics and overall TCE removal efficiency. These results were then compared to the performance of the prototype photoreactor evaluated experimentally in this research.

Figure 7, Design A, shows the CFD modeling of TCE concentration along the length of the annular prototype photoreactor and the TCE deposition rate on the photocatalyst surface. Clearly, the concentration is higher on the left-hand side of the UV lamp, opposite the inlet. This could be explained by the nonuniform flow distribution in the reactor. On the opposite side of the inlet, the flow rate is considerably higher because the inlet position leads the flow to one side of the reactor. This results in a higher gas velocity, which shortens residence time and produces a higher TCE concentration in these regions. The deposition rate on the surface of the photocatalyst is also higher on the left-hand side, where the gas flow rate is higher. In an attempt to influence these reactor hydrodynamics, the reactor inlet position was changed from perpendicular (Design A) to parallel (Design B) to the reactor length. As shown in Figure 7, Design B produces significant changes in the concentration distribution along the reactor. Also, the deposition rate at the surface of the photocatalyst (that is, along the reactor wall) became more uniform (Figure 7, Design B). The overall reactor performance, however, was not significantly improved, increasing only slightly from 67 to 69% (Table 1). This could be the result of a balance between the two factors associated with Design B. On the one hand, less mixing and lower diffusion of TCE to the surface of photocatalysts have a negative impact on the overall degradation of TCE (disadvantages of configuration B to A). On the other hand, more uniform flow distribution and optimum use of the photocatalyst in all regions of the photoreactor bring about a positive impact on TCE degradation (advantages of configuration B to A). Despite their similar performances, Design B has some advantages for the long-term operation of the photoreactor. This design results in a more uniform shear stress on the photocatalyst surface, which could be important if photocatalyst stability is an issue, such as in situations where the coated photocatalyst is prone to shear stress and abrasion. Furthermore, Design B provides a more uniform deposition/adsorption, which could be of consideration during the treatment of some organic compounds (such as

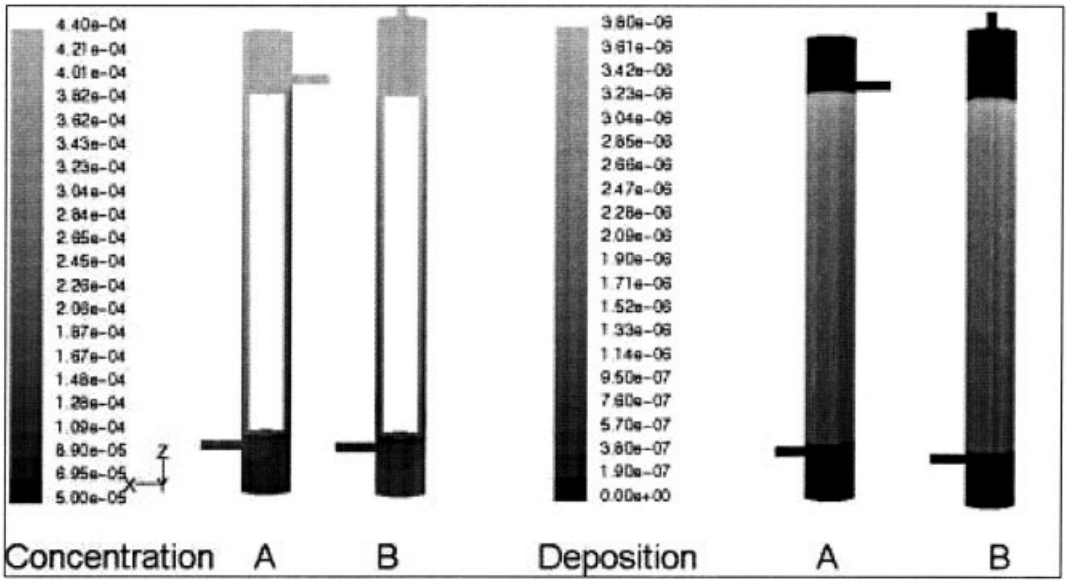

Figure 7. CFD modeling of contours of mass fraction and surface deposition rate (kg m^{-2} s^{-1}) of TCE for the cross-flow inlet (A) and parallel-flow inlet (B) photoreactors (flow rate 1.33 × 10^{-4} m^3 s^{-1}; inlet concentration 0.54 g m^{-3}).

Inlet is on top of the photoreactor (Z+ direction). There is no photocatalyst in the areas where the deposition rate is zero (at the top and bottom of the photoreactors).

aromatics) that form polymeric intermediates that inactivate the photocatalyst. Finally, uniform flow through the reactor results in a more consistent use of the photocatalyst, which could also be regenerated more effectively/consistently upon inactivation.

In Figure 8, Design A depicts CFD modeling of mass fraction of TCE at the prototype photoreactor cross section, located 0.085 m from the reactor inlet (flow rate 1.33 × 10^{-4} m^3 s^{-1}, inlet concentration 0.54 g m^{-3}). The results show that TCE concentration is not symmetric in the reactor cross section and that the overall concentration is higher at the opposite side of the inlet (the left-hand side), where there is a higher gas flow rate and shorter local residence time. Design A also shows a radial concentration gradient between the outer and inner surfaces of the reactor with lower concentration at the outer surface of the reactor, where the photocatalyst is present in the form of coating on the reactor wall. This concentration gradient is anticipated because TCE degradation takes place only on the surface of the TiO_2 photocatalyst. Therefore, changing the contaminated air layer flowing over the photocatalyst surface, by altering the distance between the lamp sleeve and the photocatalyst surface, could provide more uniform radial concentration distribution and potentially improve reactor performance.

Two other designs were simulated by changing the diameter of the photoreactor sleeve (from 23 to 27.5 and 14 mm) to increase/decrease the air layer by a factor of 2 (from 4.5 mm in Design A, to 9.0 mm in Design C, and to 2.25 mm in Design D). In all the design alternatives, the inlet flow rate and TCE concentration remained the same (flow rate 1.33 × 10^{-4} m^3 s^{-1}, inlet concentration 0.54 g m^{-3}). Also, the photoreactor diameter and, in turn, the photocatalyst surface area, remained unchanged. Figure 8 illustrates that a thicker air layer (Design C) creates a nonuniform concentration distribution, but with a thinner air layer (Design D), the concentration distribution is more uniform in the photoreactor cross section. In addition, as the air layer in the photoreactor decreases (Designs C, A, and D, respectively), the radial concentration gradient becomes more uniform. This results in an increase in the diffusion rate of the chemicals to the photocatalyst surface and, thus, enhancement in the efficiency of the catalyst for eliminating the contaminant of interest. The CFD modeling results (Table 1) predict an improvement in the photoreactor performance (from 67 to 75% degradation) as a result of reducing the air layer by a factor of 2 (from 4.5 mm in Design A to 2.25 mm in Design D). This improvement, predicted by CFD, was substantiated by preliminary experiments that showed the rate of TCE removal increased by almost 150% when the air layer was decreased by a factor of 3 in a separator flat-plate reactor configuration. Although this experiment was performed in a different reactor configuration, the preliminary test proved that smaller air lay-

Table 1. Reactor Performance at Various Conceptual Designs*

Design	Description	TCE Mass Fraction Outlet/Inlet	TCE Removal (%)
A	Inlet cross flow, air layer 4.5 mm	$1.5 \times 10^{-4}/4.4 \times 10^{-4}$	67
B	Inlet parallel flow, air layer 4.5 mm	$1.4 \times 10^{-4}/4.4 \times 10^{-4}$	69
C	Inlet cross flow, air layer 9.0 mm	$1.9 \times 10^{-4}/4.4 \times 10^{-4}$	56
D	Inlet cross flow, air layer 2.25 mm	$1.1 \times 10^{-4}/4.4 \times 10^{-4}$	75

*The performance is reported in terms of the outlet/inlet TCE mass fraction and the TCE removal (flow rate 1.33 × 10^{-4} m^3 s^{-1}).

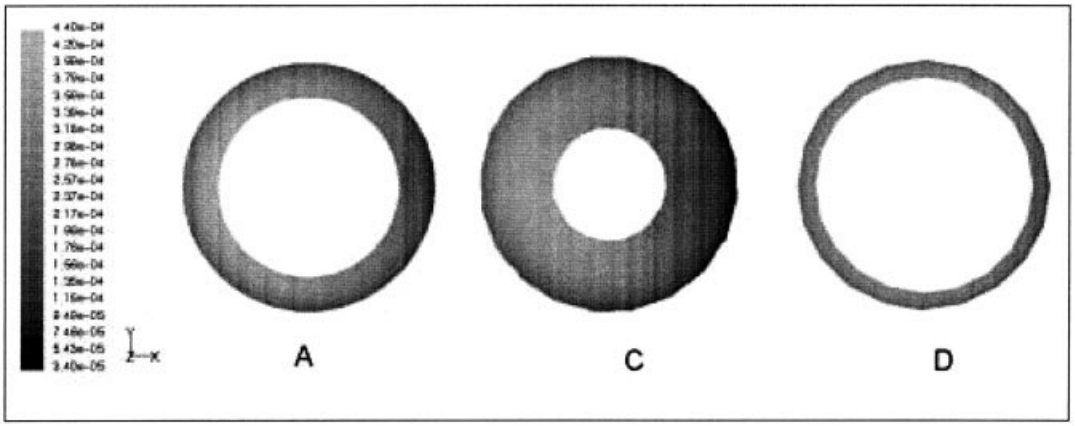

Figure 8. CFD modeling of contours of mass fraction of TCE at the reactor cross section (0.085 m from the inlet) for the 4.5-mm (A), 9-mm (B), and 2.25-mm (C) air layer photoreactors (flow rate 1.33 × 10^{-4} m^3 s^{-1}; inlet concentration 0.54 g m^{-3}).

Cross flow inlet is from the right-hand side of the photoreactor, resulting in higher flow rate and concentration on the left-hand side (see Figure 7A for the overall geometry).

ers can increase the removal rate. Although narrowing the air layer will increase the pressure drop, it is anticipated that the greater reactor performance will compensate for this disadvantage. Reaching an optimal air layer might be achieved by considering a balance between the highest possible removal rates at an appropriate pressure drop.

Conclusions

Photocatalytic oxidation of TCE followed first-order oxidation kinetics for the range of TCE concentrations between 0.1 and 1.6 g m^{-1}. CFD modeling of a photocatalytic reactor with surface reaction for TCE oxidation at various reactor lengths, pollutant concentrations, and flow rates predicted the experimental data well. CFD modeling of the annular photocatalytic reactor provided detailed information on concentration gradients of the contaminant in the reactor and provided accurate analysis and explanation of the experimental results. Improvement in photoreactor performance could be achieved by using the information provided by modeling. CFD modeling demonstrated that under similar flow rate conditions, the thickness of contaminated air flow (the contaminated air layer flowing over the photocatalyst surface) influences the reactor performance. A thinner contaminated air layer provided more uniform radial concentration distribution of TCE and improved the reactor performance, within the range of air layers (2.25–9.0 mm) and flow rates (1.33 × 10^{-4} m^3 s^{-1}) examined.

Acknowledgments

The authors acknowledge financial support from the Natural Sciences and Engineering Research Council of Canada (NSERC), Canada Foundation for Innovation (CFI) New Opportunity Fund, and British Columbia Knowledge Development Fund (BCKDF).

Notation

ρ = density, kg m^{-3}
$\bar{\bar{\tau}}$ = stress tensor, N m^{-2}
$v'_{i,r}$ = stoichiometric coefficient for reactant i in reaction r
$v''_{i,r}$ = stoichiometric coefficient for product i in reaction r
$\eta_{j,r}$ = forward rate exponent for each reactant and product species j in reaction r
$C_{j,r}$ = molecular concentration of each reactant and product species j in reaction r, kg m^{-2} s^{-1}
g = gravitational force, m s^{-2}
$\vec{J}_i$ = diffusion flux of species i, kg m^{-2} s^{-1}
k = first-order surface reaction rate constant, m^3 m^{-2} s^{-1}
M_i = symbol denoting species i
$M_{w,i}$ = molar weight of the species i, kg $kmol^{-1}$
N = total number of species in the system
P = pressure, N m^{-2}
r = photocatalytic reaction rate, g m^{-2} min^{-1}
R_i = rate of production or depletion of species i arising from volumetric reactions, kg m^{-3} s^{-1}
R_i^s = rate of surface production or depletion of species i, kg m^{-2} s^{-1}
$R_{i,r}^s$ = rate of molar production or depletion of species i, kmol m^{-2} s^{-1}
$\vec{v}$ = velocity, m s^{-1}
Y_i = species i

Literature Cited

1. Alfano OM, Behnemann D, Cassano AE, Dillert R, Goslich R. Photocatalysis in water environments using artificial and solar light. *Catal Today.* 2000;58:199-230.
2. Dibble LA, Raupp GB. Fluidized-bed photocatalytic oxidation of trichloroethylene in contaminated air streams. *Environ Sci Technol.* 1992;26:492-495.
3. Mohseni M, David A. Gas phase vinyl chloride (VC) oxidation using TiO_2 based photocatalysis. *Appl Catal B Environ.* 2003;46:219-228.
4. Raupp GB, Nico JA, Annangi S, Changrani R, Annapragada R. Two-flux radiation-field model for an annular packed-bed photocatalytic oxidation reactor. *AIChE J.* 1997;43:792-801.
5. Hossain MM, Raupp GB. Radiation field modeling in a photocatalytic monolith reactor. *Chem Eng Sci.* 1998;53:3771-3780.
6. Lim TK, Kim SD. Trichloroethylene by photocatalysis in annular flow and annulus fluidized bed photoreactors. *Chemosphere.* 2004;54:305-312.
7. Pareek VK, Adesina AA. Analysis of photocatalytically reactive systems: Kinetic modeling and reactor design via computational fluid dynamics. In: Nalwa HS, ed. *Handbook of Photochemistry and Photobiology*. Stevenson Ranch, CA: American Scientific Publishers; 2003:345-412.
8. Mohseni M, Taghipour F. Experimental and CFD analysis of photo-

catalytic gas phase vinyl chloride (VC) oxidation. *Chem Eng Sci.* 2004;59:1601-1609.
9. Hjertager LK, Hjertager BH, Solberg T. CFD modelling of fast chemical reactions in turbulent liquid flows. *Comput Chem Eng.* 2002;26: 507-515.
10. van Baten JM, Ellenberger J, Krishna R. Scale-up strategy for bubble column slurry reactors using CFD simulations. *Catal Today*. 2003;79/ 80:259-265.
11. Marchisio DL, Barresi AA. CFD simulation of mixing and reaction: The relevance of the micro-mixing model. *Chem Eng Sci.* 2003;58: 3579-3587.
12. Gamwo IK, Halow JS, Gidaspow D, Mostofi D. CFD models for methanol synthesis three-phase reactors: Reactor optimization. *Chem Eng J.* 2003;93:103-112.
13. Kucuk Unluturka S, Arastoopour H, Koutchma T. Modeling of UV dose distribution in a thin-film UV reactor for processing of apple cider. *J Food Eng.* 2004;65:125-136.
14. Taghipour F, Elyasi S, Sozzi A. Simulation of ozone-UV reactors for water treatment (Water Environment Management Series). Proc of 2nd IWA Leading-Edge Conf on Water and Wastewater Treatment Technologies, Prague, Czech Republic, 2004. Water Intelligence Online ©IWA Publishing. London: International Water Association; 2005.
15. Taghipour F. Development of a CFD-based model for photo-reactor simulation. *Parallel Computational Fluid Dynamics*. London, UK: Elsevier Science; 2004:243-250.
16. Endo H, Kuwana K, Saito K, Qian D, Andrews R, Grulke EA. CFD prediction of carbon nanotube production rate in a CVD reactor. *Chem Phys Lett.* 2004;387:307-311.
17. Seo YS, Yu SP, Cho SJ, Song KS. The catalytic heat exchanger using catalytic fin tubes. *Chem Eng Sci.* 2003;58:43-53.
18. Heitsch M. Fluid dynamic analysis of a catalytic recombiner to remove hydrogen. *Nucl Eng Des.* 2000;201:1-10.
19. *Fluent User's Manual*. Lebanon, NH: Fluent Inc.; 2002.
20. Hubrich C, Stuhl F. The ultraviolet absorption of some halogenated methanes and ethanes of atmospheric interests. *J Photochem.* 1980; 12:93-107.
21. Keshmiri M, Mohseni M, Troczynski T. Development of novel TiO_2 sol-gel-derived composite and its photocatalytic activities for trichloroethylene oxidation. *Appl Catal B Environ.* 2004;53:209-219.
22. Upadhya S, Ollis DF. A simple kinetic model for the simultaneous concentration and intensity dependence of TCE photocatalyzed destruction. *J Adv Oxidat Technol.* 1998;3:199-202.

Manuscript received Sep. 12, 2004, and revision received Mar. 1, 2005.